Stanford Exploration Project, Report 114, October 14, 2003, pages 1–31

Seismic imaging using Riemannian wavefield extrapolation

Paul Sava and Sergey Fomel[1]

ABSTRACT

Riemannian spaces are described by non-orthogonal curvilinear coordinates. We generalize one-way wavefield extrapolation to semi-orthogonal Riemannian coordinate systems, which include, but are not limited to, ray coordinate systems. We obtain one-way wavefield extrapolation methods which are not dip-limited, and which can even be used to image overturning waves. Ray coordinate systems can be initiated either from point sources, or from plane waves incident at various angles. Since wavefield propagation happens mostly along the extrapolation direction, we can use cheap finite-difference or mixed-domain extrapolators to achieve high angle accuracy. The main applications of our method include imaging of steeply dipping or overturning reflections.

INTRODUCTION

Imaging complex geology is one of the main challenges of today's seismic processing. Of the many seismic imaging methods available, downward continuation (Claerbout, 1985) has proven to be accurate, robust, and capable of handling models with large and sharp velocity variations. In addition, such methods naturally handle the multipathing which occurs in complex geology and provide a band-limited solution to the seismic imaging problem. Furthermore, as computational power increases, such methods are gradually moving into the mainstream of seismic processing.

However, migration by downward continuation imposes strong limitations on the dip of reflectors that can be imaged since, by design, it favors energy which is propagating mainly in the downward direction. Upward propagating energy, e.g., overturning waves, can be imaged in principle using downward continuation methods (Hale et al., 1992), although the procedure is difficult, particularly for prestack data. In contrast, Kirchhoff-type methods based on ray-traced traveltimes can image steep dips and handle overturning waves, although those methods are far less reliable in complex environments given their high-frequency asymptotic nature.

The steep-dip limitation of downward continuation techniques has been addressed in several ways:

- A first option is to increase the angular accuracy of the extrapolation operator, for example by employing methods from the Fourier finite-difference (FFD) family (Ristow

[1]**email:** paul@sep.stanford.edu, sergey.fomel@beg.utexas.edu

and Ruhl, 1994; Biondi, 2002), or the Generalized Screen Propagator (GSP) family (de Hoop, 1996; Huang and Wu, 1996). The enhancements brought about by these methods come at a price, since they increase the cost of extrapolation without guaranteeing unconditional stability.

- A second option is to perform the wavefield extrapolation in tilted coordinate systems (Etgen, 2002), or by designing sources which favor illumination of particular regions of the image (Rietveld and Berkhout, 1994; Chen et al., 2002). We can thus increase angular accuracy, although those methods favor a subset of the model (a salt flank, for example), while potentially decreasing the accuracy in other regions. In complex models it is also not obvious what is an optimal tilt angle for the extrapolation grid.

- A third possibility is hybridization of wavefield and ray-based techniques, either in the form of Gaussian beams (Hill, 1990, 2001; Gray et al., 2002), coherent states (Albertin et al., 2001, 2002), or beam-waves (Brandsberg-Dahl and Etgen, 2003). Such techniques are quite powerful, since they couple wavefield methods with multipathing and band-limited properties, with ray methods, which deliver arbitrary directions of propagation, even overturning. The main strength of those techniques, is also their main weakness, i.e. they are formulated in terms of decoupled beams. Beams may leave shadow zones in various parts of the model, which hamper their imaging abilities. Furthermore, beams have limited size, which in turn limits the extent of the diffractions created by sharp features in the model to that of any particular beam, no matter how accurate the extrapolator within each beam is. In addition, the narrow extrapolation domain poses serious beam superposition problems, such as beam boundary effects.

The main idea of our paper is to couple the beams together and extrapolate within all of them at once. We, therefore, cannot talk about beams anymore, but instead we need to talk about continuously changing coordinate systems. We extend downward continuation in a regular Cartesian space to wavefield extrapolation in distorted coordinates, known as *Riemannian spaces*, thus the name of our method. We formulate the theory in arbitrary 3-D semi-orthogonal Riemannian spaces, e.g., ray coordinates, although those coordinate systems do not necessarily need to have a physical meaning as long as they fulfill the semi-orthogonality condition. Examples of such coordinate systems include, but are not limited to, fans of rays emerging from a source point, or bundles of rays initiated by plane waves of arbitrary initial dips at the source. A special case of our method is represented by the polar/spherical coordinate system (Nichols and Palacharla, 1994; Nichols, 1994, 1996).

Our method can be seen as a finite-difference solution to the acoustic wave-equation in ray coordinates. In this respect, it is closely related to Huygens wavefront tracing (Sava and Fomel, 2001), which represents a finite-difference solution to the eikonal equation in ray coordinates.

Another idea related to our method is that of wave-equation in ray-centered coordinates (Yedlin, 1981; Červený, 2001). However, our method is different since the ray-centered coordinate system is orthogonal in 3-D and defined around an individual ray. In contrast, our method is formulated in ray coordinates which are parameterizations of the wavefields at the source, and which are non-orthogonal in 3-D and defined globally for an entire family of rays.

The upside of our method is that the coordinate system may follow the waves, and can even overturn, such that we can use one-way extrapolators to image diving waves (Figure 1). We can also use extrapolators with small angle accuracy (e.g. 15°), since, in principle, we are

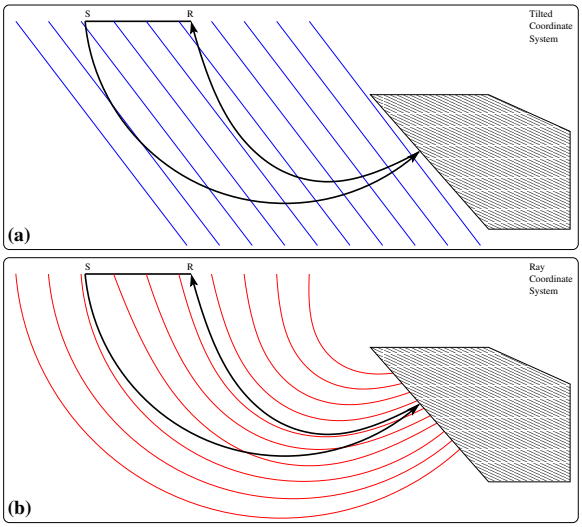

Figure 1: Ray coordinate systems are superior to tilted coordinate systems for imaging overturning waves using one-way wavefield extrapolators. Overturning reflected energy may become evanescent in tilted coordinate systems (a), but stays non-evanescent in ray coordinate systems (b). paul2-overturned [NR]

never too far from the actual direction in which waves propagate. We are also not confined to the extent of any individual beam, therefore we can track diffractions for their entire spatial extent.

ACOUSTIC WAVE-EQUATION IN 3-D RIEMANNIAN SPACES

The Laplacian operator of a scalar function $\mathcal{U}$ in an arbitrary Riemannian space with coordinates $\{\xi_1,\xi_2,\xi_3\}$ has the form

$$\Delta\mathcal{U} = \sum_{i=1}^{3} \frac{1}{\sqrt{|\mathbf{g}|}} \frac{\partial}{\partial \xi_i} \left(\sum_{j=1}^{3} g^{ij} \sqrt{|\mathbf{g}|} \frac{\partial \mathcal{U}}{\partial \xi_j} \right), \tag{1}$$

where g^{ij} is a component of the associated metric tensor, and $|\mathbf{g}|$ is its determinant (Synge and Schild, 1978).

The expression simplifies if one of the coordinates (e.g. the coordinate of one-way wave extrapolation) is orthogonal to the other coordinates. Let $\xi_1 = \xi$, $\xi_2 = \eta$, and $\xi_3 = \zeta$, with ζ orthogonal to both ξ and η. Then the metric tensor has the matrix

$$\left[g_{ij}\right] = \begin{bmatrix} E & F & 0 \\ F & G & 0 \\ 0 & 0 & \alpha^2 \end{bmatrix}, \tag{2}$$

where E, F, G, and α are differential forms that can be found from mapping Cartesian coordinates $\mathbf{x}$ to the general coordinates $\{\xi,\eta,\zeta\}$, as follows:

$$E \;=\; \mathbf{x}_\xi \cdot \mathbf{x}_\xi \;,$$

$$\begin{aligned} F &= \mathbf{x}_\xi \cdot \mathbf{x}_\eta \,, \\ G &= \mathbf{x}_\eta \cdot \mathbf{x}_\eta \,, \\ \alpha^2 &= \mathbf{x}_\zeta \cdot \mathbf{x}_\zeta \,. \end{aligned} \tag{3}$$

The associated metric tensor has the matrix

$$\left[g^{ij}\right] = \begin{bmatrix} +G/J^2 & -F/J^2 & 0 \\ -F/J^2 & +E/J^2 & 0 \\ 0 & 0 & 1/\alpha^2 \end{bmatrix}, \tag{4}$$

where $J^2 = E\,G - F^2$. The metric determinant takes the form

$$|\mathbf{g}| = \alpha^2 J^2 \,. \tag{5}$$

Substituting equations (4) and (5) into (1), we can modify the Helmholtz wave equation

$$\Delta \mathcal{U} = -\frac{\omega^2}{v^2(\mathbf{x})}\mathcal{U}$$

for propagating waves in a 3-D Riemannian space:

$$\frac{1}{\alpha J}\left[\frac{\partial}{\partial \zeta}\left(\frac{J}{\alpha}\frac{\partial \mathcal{U}}{\partial \zeta}\right) + \frac{\partial}{\partial \xi}\left(G\frac{\alpha}{J}\frac{\partial \mathcal{U}}{\partial \xi} - F\frac{\alpha}{J}\frac{\partial \mathcal{U}}{\partial \eta}\right) + \frac{\partial}{\partial \eta}\left(E\frac{\alpha}{J}\frac{\partial \mathcal{U}}{\partial \eta} - F\frac{\alpha}{J}\frac{\partial \mathcal{U}}{\partial \xi}\right)\right] = -\frac{\omega^2}{v^2}\mathcal{U} \,. \tag{6}$$

In equation (6), ω is temporal frequency, $v\,[\mathbf{x}(\xi,\eta,\zeta)]$ is the wave propagation velocity, and $\mathcal{U}$ represents a propagating wave.

For the special case of two dimensional spaces ($F = 0$ and $G = 1$), the Helmholtz wave equation reduces to the simpler form:

$$\frac{1}{\alpha J}\left[\frac{\partial}{\partial \zeta}\left(\frac{J}{\alpha}\frac{\partial \mathcal{U}}{\partial \zeta}\right) + \frac{\partial}{\partial \xi}\left(\frac{\alpha}{J}\frac{\partial \mathcal{U}}{\partial \xi}\right)\right] = -\frac{\omega^2}{v^2}\mathcal{U} \,, \tag{7}$$

which corresponds to a curvilinear orthogonal coordinate system.

Particular examples of coordinate systems for one-way wave propagation are:

Cartesian (propagation in depth): $x_1 = \xi, x_2 = \eta, x_3 = \zeta$,

$$\begin{aligned} E &= G = \alpha = J = 1 \,, \\ F &= 0 \,. \end{aligned}$$

Cylindrical (propagation in radius): $x_1 = \zeta\,\cos\xi, x_2 = \zeta\,\sin\xi, x_3 = \eta$,

$$\begin{aligned} E &= J = \zeta^2 \,, \\ G &= \alpha = 1 \,, \\ F &= 0 \,. \end{aligned}$$

Spherical (propagation in radius): $x_1 = \zeta \sin\xi \cos\eta$, $x_2 = \zeta \sin\xi \sin\eta$, $x_3 = \zeta \cos\xi$,

$$\begin{aligned} E &= \zeta^2 \,, \\ G &= \zeta^2 \sin^2\xi \,, \\ \alpha &= 1 \,, \\ J &= \zeta^2 \sin\xi \,, \\ F &= 0 \,. \end{aligned}$$

Ray family (propagation along rays): ξ and η represent parameters defining a particular ray in the family (i.e. the ray take-off angles), J is the geometrical spreading factor, related to the cross-sectional area of the ray tube (Červený, 2001). The coefficients E, F, G, and J are easily computed by finite-difference approximations with the Huygens wavefront tracing technique (Sava and Fomel, 2001). If the propagation parameter ζ is taken to be time along the ray, then α equals the propagation velocity v.

ONE-WAY WAVE-EQUATION IN 3-D RIEMANNIAN SPACES

Equation (6) can be used to describe two-way propagation of acoustic waves in a semi-orthogonal Riemannian space. For one-way wavefield extrapolation, we need to modify the acoustic wave equation (6) by selecting a single direction of propagation.

In order to simplify the computations, we introduce the following notation:

$$\begin{aligned} c_{\zeta\zeta} &= \frac{1}{\alpha^2} \,, \\ c_{\xi\xi} &= \frac{G}{J^2} \,, \\ c_{\eta\eta} &= \frac{E}{J^2} \,, \\ c_{\xi\eta} &= \frac{F}{J^2} \,, \\ c_{\zeta} &= \frac{1}{\alpha J} \frac{\partial}{\partial \zeta} \left(\frac{J}{\alpha} \right) \,, \\ c_{\xi} &= \frac{1}{\alpha J} \left[\frac{\partial}{\partial \xi} \left(G \frac{\alpha}{J} \right) - \frac{\partial}{\partial \eta} \left(F \frac{\alpha}{J} \right) \right] \,, \\ c_{\eta} &= \frac{1}{\alpha J} \left[\frac{\partial}{\partial \eta} \left(E \frac{\alpha}{J} \right) - \frac{\partial}{\partial \xi} \left(F \frac{\alpha}{J} \right) \right] \,. \end{aligned} \tag{8}$$

All quantities in equations (8) can be computed by finite-differences for any choice of a Riemannian coordinate system which fulfills the orthogonality condition indicated earlier. In particular, we can use ray coordinates to compute those coefficients. With these notations, the acoustic wave-equation can be written as:

$$c_{\zeta\zeta} \frac{\partial^2 \mathcal{U}}{\partial \zeta^2} + c_{\xi\xi} \frac{\partial^2 \mathcal{U}}{\partial \xi^2} + c_{\eta\eta} \frac{\partial^2 \mathcal{U}}{\partial \eta^2} + c_{\zeta} \frac{\partial \mathcal{U}}{\partial \zeta} + c_{\xi} \frac{\partial \mathcal{U}}{\partial \xi} + c_{\eta} \frac{\partial \mathcal{U}}{\partial \eta} + c_{\xi\eta} \frac{\partial^2 \mathcal{U}}{\partial \xi \partial \eta} = -\frac{\omega^2}{v^2} \mathcal{U} \,. \tag{9}$$

For the particular case of Cartesian coordinates ($c_\xi = c_\eta = c_\zeta = 0, c_{\xi\xi} = c_{\eta\eta} = c_{\zeta\zeta} = 1, c_{\xi\eta} = 0$), the Helmholtz equation (9) takes the familiar form

$$\frac{\partial^2 \mathcal{U}}{\partial \zeta^2} + \frac{\partial^2 \mathcal{U}}{\partial \xi^2} + \frac{\partial^2 \mathcal{U}}{\partial \eta^2} = -\frac{\omega^2}{v^2}\mathcal{U} \,. \tag{10}$$

From equation (9), we can directly deduce the modified form of the dispersion relation for the wave-equation in a semi-orthogonal 3-D Riemannian space:

$$-c_{\zeta\zeta}k_\zeta^2 - c_{\xi\xi}k_\xi^2 - c_{\eta\eta}k_\eta^2 + ic_\zeta k_\zeta + ic_\xi k_\xi + ic_\eta k_\eta - c_{\xi\eta}k_\xi k_\eta = -\omega^2 s^2 \,. \tag{11}$$

For one-way wavefield extrapolation, we need to solve the second order equation (11) for the wavenumber of the extrapolation direction k_ζ, and select the solution with the appropriate sign to extrapolate waves in the desired direction:

$$k_\zeta = i\frac{c_\zeta}{2c_{\zeta\zeta}} \pm \sqrt{\frac{(\omega s)^2}{c_{\zeta\zeta}} - \left(\frac{c_\zeta}{2c_{\zeta\zeta}}\right)^2 - \left[\frac{c_{\xi\xi}}{c_{\zeta\zeta}}k_\xi^2 - i\frac{c_\xi}{c_{\zeta\zeta}}k_\xi\right] - \left[\frac{c_{\eta\eta}}{c_{\zeta\zeta}}k_\eta^2 - i\frac{c_\eta}{c_{\zeta\zeta}}k_\eta\right] - \frac{c_{\xi\eta}}{c_{\zeta\zeta}}k_\xi k_\eta} \,. \tag{12}$$

The solution with the positive sign in equation (12) corresponds to propagation in the positive direction of the extrapolation axis ζ.

For the particular case of Cartesian coordinates ($c_\xi = c_\eta = c_\zeta = 0, c_{\xi\xi} = c_{\eta\eta} = c_{\zeta\zeta} = 1, c_{\xi\eta} = 0$), the one-way wavefield extrapolation equation takes the familiar form

$$k_\zeta = \pm\sqrt{(\omega s)^2 - k_\xi^2 - k_\eta^2} \,. \tag{13}$$

MIXED-DOMAIN SOLUTIONS TO THE ONE-WAY WAVE-EQUATION

We can use equation (12) to construct a numerical solution to the one-way wave equation in the mixed $\omega - k$, $\omega - x$ domain. The extrapolation wavenumber described in equation (12) is, in general, a function which depends on several quantities

$$k_\zeta = k_\zeta\left(s, c_j\right) \,, \tag{14}$$

where $s\left(\zeta,\xi,\eta\right)$ is the space-variable slowness, and $c_j\left(\zeta,\xi,\eta\right) = \left\{c_\xi, c_\eta, c_\zeta, c_{\xi\xi}, c_{\eta\eta}, c_{\zeta\zeta}, c_{\xi\eta}\right\}$ are coefficients which are computed numerically from the definition of the coordinate system, as indicated by equations (8). For any given coordinate system, c_j can be regarded as known.

Next, we write the extrapolation wavenumber k_ζ as a first-order Taylor expansion relative to a reference medium:

$$k_\zeta = k_{\zeta 0} + \left.\frac{\partial k_\zeta}{\partial s}\right|_{s_0, c_{j0}} (s - s_0) + \sum_{c_j} \left.\frac{\partial k_\zeta}{\partial c_j}\right|_{s_0, c_{j0}} \left(c_j - c_{j0}\right) \,, \tag{15}$$

where $s\left(\zeta,\xi,\eta\right)$ and $c_j\left(\zeta,\xi,\eta\right)$ represent the spatially variable slowness and coordinate system parameters, and s_0 and c_{j0} are the constant reference values in every extrapolation "slab" (Sava, 2000).

As usual, the first part of equation (15), corresponding to the extrapolation wavenumber in the reference medium $k_{\zeta 0}$, is implemented in the Fourier domain, while the second part, corresponding to the spatially variable medium coefficients, is implemented in the space domain.

If we make the further simplifying assumptions that $k_\xi \approx 0$ and $k_\eta \approx 0$, we can write

$$k_\zeta = k_{\zeta 0} + \left.\frac{\partial k_\zeta}{\partial c_{\zeta\zeta}}\right|_0 (s - s_0) + \left.\frac{\partial k_\zeta}{\partial c_{\zeta\zeta}}\right|_0 \left(c_{\zeta\zeta} - c_{\zeta\zeta 0}\right) + \left.\frac{\partial k_\zeta}{\partial c_\zeta}\right|_0 \left(c_\zeta - c_{\zeta 0}\right) \ , \tag{16}$$

where

$$\begin{aligned}
\left.\frac{\partial k_\zeta}{\partial s}\right|_0 &= \frac{2\omega(\omega s_0)}{\sqrt{4c_{\zeta\zeta 0}(\omega s_0)^2 - c_{\zeta 0}^2}} \\
\left.\frac{\partial k_\zeta}{\partial c_{\zeta\zeta}}\right|_0 &= -\frac{i c_{\zeta 0}}{2c_{\zeta\zeta 0}^2} + \frac{c_{\zeta 0}^2 - 2c_{\zeta\zeta 0}(\omega s_0)^2}{2c_{\zeta\zeta 0}^2\sqrt{4c_{\zeta\zeta 0}(\omega s_0)^2 - c_{\zeta 0}^2}} \\
\left.\frac{\partial k_\zeta}{\partial c_\zeta}\right|_0 &= \frac{i}{2c_{\zeta\zeta 0}} - \frac{c_{\zeta 0}}{2c_{\zeta\zeta 0}\sqrt{4c_{\zeta\zeta 0}(\omega s_0)^2 - c_{\zeta 0}^2}} \ .
\end{aligned} \tag{17}$$

Equation (16) is motivated by a wavefront normal propagation approximation. By "0", we denote the reference medium (s_0, c_{j0}). We could also use many reference media, followed by interpolation, similarly to the technique of Gazdag and Sguazzero (1984).

For the particular case of Cartesian coordinates ($c_\zeta = 0, c_{\zeta\zeta} = 1$), equation (16) reduces to

$$k_\zeta = k_{\zeta 0} + \omega(s - s_0) \ , \tag{18}$$

which corresponds to the popular Split-Step Fourier (SSF) extrapolation method (Stoffa et al., 1990).

FINITE-DIFFERENCE SOLUTIONS TO THE ONE-WAY WAVE EQUATION

Alternative solutions to the one-way wave-equation are represented by pure finite-difference methods in the $\omega - x$ domain, which can be implemented either as implicit (Claerbout, 1985), or as explicit methods (Hale, 1991). For the same stencil size, the implicit methods are more accurate and robust than explicit methods, although harder to implement, particularly in 3-D. However, explicit methods of comparable accuracy can be designed using larger stencils.

For the implicit methods, various approximations to the square root in equation (12) lead to approximate equations of various orders of accuracy. In the Cartesian space, those methods are known by their respective angular accuracy as the 15° equation, 45° equation and so on. Although the meanings of 15°, 45° are undefined in ray coordinates where the extrapolation axis is time, we can still write approximations for the numerical finite-difference solutions using analogous approximations.

If we introduce the notation

$$k_o^2 = \frac{(\omega s)^2}{c_{\zeta\zeta}} - \left(\frac{c_\zeta}{2c_{\zeta\zeta}}\right)^2 \tag{19}$$

we can simplify the one-way wave equation (12) as

$$k_\zeta = i\frac{c_\zeta}{2c_{\zeta\zeta}} + \sqrt{k_o^2 - \left[\frac{c_{\xi\xi}}{c_{\zeta\zeta}}k_\xi^2 - i\frac{c_\xi}{c_{\zeta\zeta}}k_\xi\right] - \left[\frac{c_{\eta\eta}}{c_{\zeta\zeta}}k_\eta^2 - i\frac{c_\eta}{c_{\zeta\zeta}}k_\eta\right] - \frac{c_{\xi\eta}}{c_{\zeta\zeta}}k_\xi k_\eta}\,. \tag{20}$$

15° wave-equation in a 3-D Riemannian space

A simple way of deriving the 15° equation is by a second order Taylor series expansion of the extrapolation wavenumber k_ζ relative to k_ξ and k_η:

$$\begin{aligned} k_\zeta\left(k_\xi,k_\eta\right) \approx k_\zeta\left(k_\xi=0,k_\eta=0\right) + \left.\frac{\partial k_\zeta}{\partial k_\xi}\right|_0 k_\xi + \left.\frac{\partial k_\zeta}{\partial k_\eta}\right|_0 k_\eta + \\ + \frac{1}{2}\left.\frac{\partial^2 k_\zeta}{\partial k_\xi^2}\right|_0 k_\xi^2 + \left.\frac{\partial^2 k_\zeta}{\partial k_\xi\,\partial k_\eta}\right|_0 k_\xi k_\eta + \frac{1}{2}\left.\frac{\partial^2 k_\zeta}{\partial k_\eta^2}\right|_0 k_\eta^2\,. \end{aligned} \tag{21}$$

If we plug equation (20) into equation (21), we obtain an equivalent form for the 15° equation in a semi-orthogonal 3-D Riemannian space:

$$\begin{aligned} k_\zeta \approx i\frac{c_\zeta}{2c_{\zeta\zeta}} + k_o + \frac{ic_\xi}{2c_{\zeta\zeta}\,k_o}k_\xi + \frac{1}{2\,k_o}\left[\left(\frac{c_\xi}{2c_{\zeta\zeta}\,k_o}\right)^2 - \frac{c_{\xi\xi}}{c_{\zeta\zeta}}\right]k_\xi^2 \\ + \frac{ic_\eta}{2c_{\zeta\zeta}\,k_o}k_\eta + \frac{1}{2\,k_o}\left[\left(\frac{c_\eta}{2c_{\zeta\zeta}\,k_o}\right)^2 - \frac{c_{\eta\eta}}{c_{\zeta\zeta}}\right]k_\eta^2 \\ + \frac{1}{2\,k_o}\left[\frac{c_\xi c_\eta}{2c_{\zeta\zeta}^2\,k_o^2} - \frac{c_{\xi\eta}}{c_{\zeta\zeta}}\right]k_\xi k_\eta\,. \end{aligned} \tag{22}$$

For the particular case of Cartesian coordinates ($c_\xi = c_\eta = c_\zeta = 0, c_{\xi\xi} = c_{\eta\eta} = c_{\zeta\zeta} = 1, c_{\xi\eta} = 0$, $k_o = \omega s$),

$$k_\zeta \approx \omega s - \frac{1}{2\omega s}\left(k_\xi^2 + k_\eta^2\right)\,, \tag{23}$$

which is the usual form of the 15° equation.

EXAMPLES

We illustrate our method with several synthetic examples of various degrees of complexity. In all examples, we use extrapolation in 2-D orthogonal Riemannian spaces (ray coordinates), and compare the results with extrapolation in Cartesian coordinates. We present images obtained by migration of synthetic datasets represented by events equally spaced in time. When

we use point sources, those images are representations of Green's functions. In all examples, (x,z) are the Cartesian space coordinates, (τ,x_0) are the ray coordinates for plane wave sources, and (τ,γ) are ray coordinates for point sources. x_0 stands for surface coordinate, γ for shooting angle, and τ for one-way traveltime.

Our first example is designed to illustrate our method in a fairly simple model. We use a 2-D model with horizontal and vertical gradients $v(x,z) = 250 + 0.2\ x + 0.15\ z$ m/s which gives waves propagating from a point source a pronounced tendency to overturn (Figure 2). The model also contains a diffractor located around $x = 3800$ m and $z = 3000$ m.

We use ray tracing to create an orthogonal ray coordinate system corresponding to a point source on the surface at $x = 6000$ m. Figure 2(a) shows the velocity model and the rays in the original Cartesian coordinate system (x,z). Figure 2(c) shows the velocity model mapped into the ray coordinate system (τ,γ). The diffractor is mapped to $\tau = 2.4$ s and $\gamma = -18°$ measured from the vertical. The synthetic data we use is represented by impulses at the source location at every 0.25 s. In ray coordinates, this source is represented by a plane-wave evenly distributed over all shooting angles γ. Ideally, an image obtained by migrating such a dataset is a representation of the acoustic wavefield produced by a source which pulsates periodically.

Figure 2(b) shows the image obtained by downward continuation in Cartesian coordinates using the standard 15° equation. Figure 2(d) shows the image obtained by wavefield extrapolation in ray coordinates using the equivalent 15° equation. The overlays in panels (b) and (d) are wavefronts at every 0.25 s and rays shot at every 20° to facilitate one-to-one comparisons between the images in ray and Cartesian coordinates.

Figure 3 is a direct comparison of the results obtained by extrapolation in the two coordinate systems. The image created by extrapolation in Cartesian coordinates (a) is mapped to ray coordinates (b). The image created by extrapolation in ray coordinates (c) is mapped to Cartesian coordinates (d). Since we use the same velocity for ray tracing and for wavefield extrapolation, we expect the wavefields and the overlain wavefronts to be in agreement. The most obvious mismatch occurs in regions where the 15° equation fails to extrapolate correctly at steep dips (around $\gamma = (-20,-50)°$. This is not surprising since, as its name indicates, this equation is only accurate up to 15°. However, this limitation is eliminated in ray coordinates, because the coordinate system brings the extrapolator in a reasonable position and at a good angle, although the extrapolator uses an equation of a similar order of accuracy.

Another interesting observation in Figures 3 (a) and (d) concerns the diffractor we introduced in the velocity model. When we extrapolate in Cartesian coordinates, the diffraction is only accurate to a small angle relative to the extrapolation direction (vertical). In contrast, the diffraction develops relative to the propagation direction when computed in ray coordinates, thus being more accurate after mapping to Cartesian coordinates.

We can also observe that the diffractions created by the anomaly in the velocity model are not at all limited in the ray coordinates domain. In a beam-type approach, such diffraction would not develop beyond the extent of any particular beam which interacts with it. Neighboring beams would be completely insensitive to the presence of the velocity anomaly.

The second example concerns a smooth velocity with a negative Gaussian anomaly which

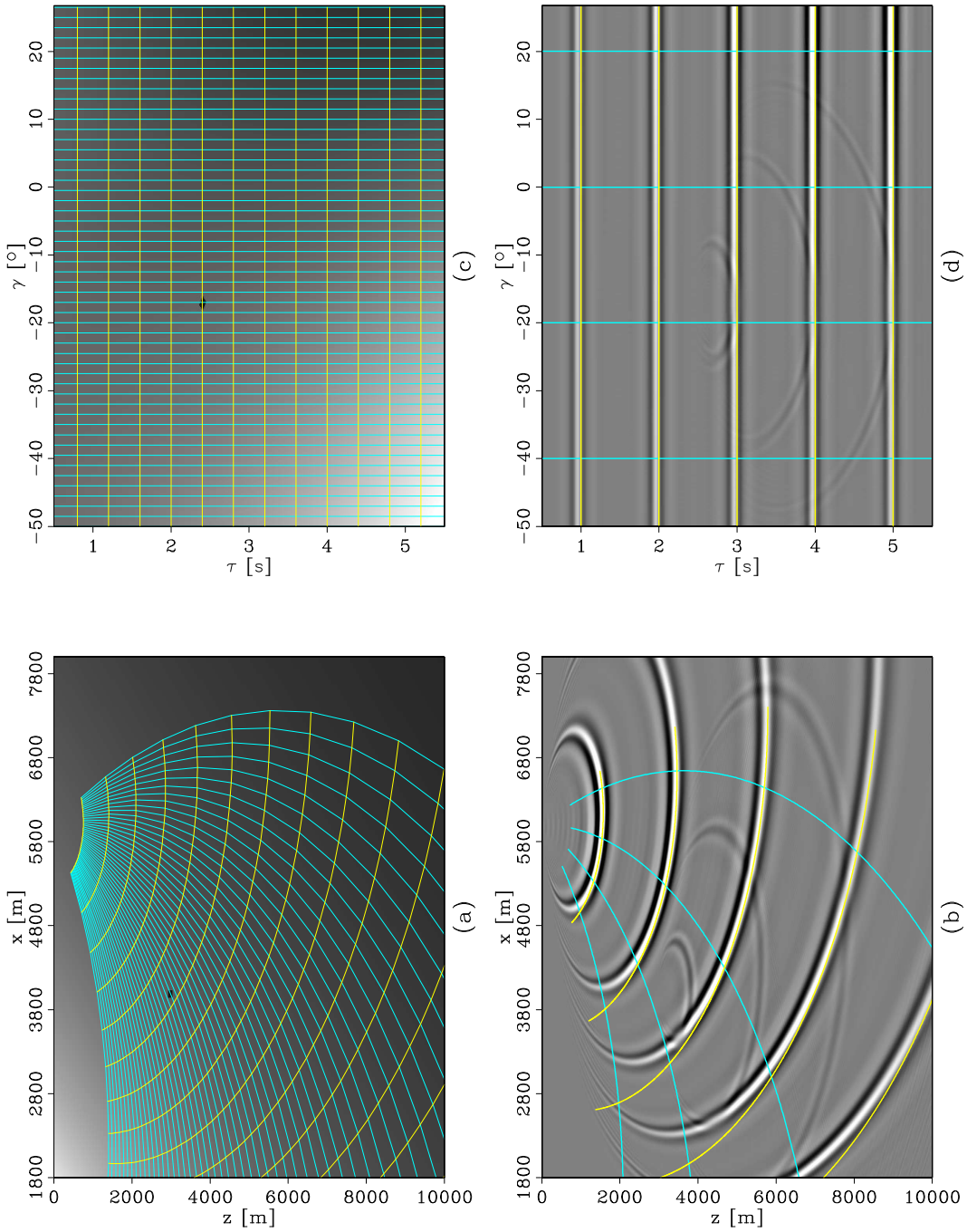

Figure 2: Simple linear gradient model: Cartesian coordinates (a,b) and ray coordinates (c,d). velocity model with an overlay of the ray coordinate system initiated by a point source at the surface (a); image obtained by downward continuation in Cartesian coordinates with the 15° equation (b); velocity model with an overlay of the ray coordinate system (c); image obtained by wavefield extrapolation in ray coordinates with the 15° equation (d). paul2-RCsim.com.ps [CR]

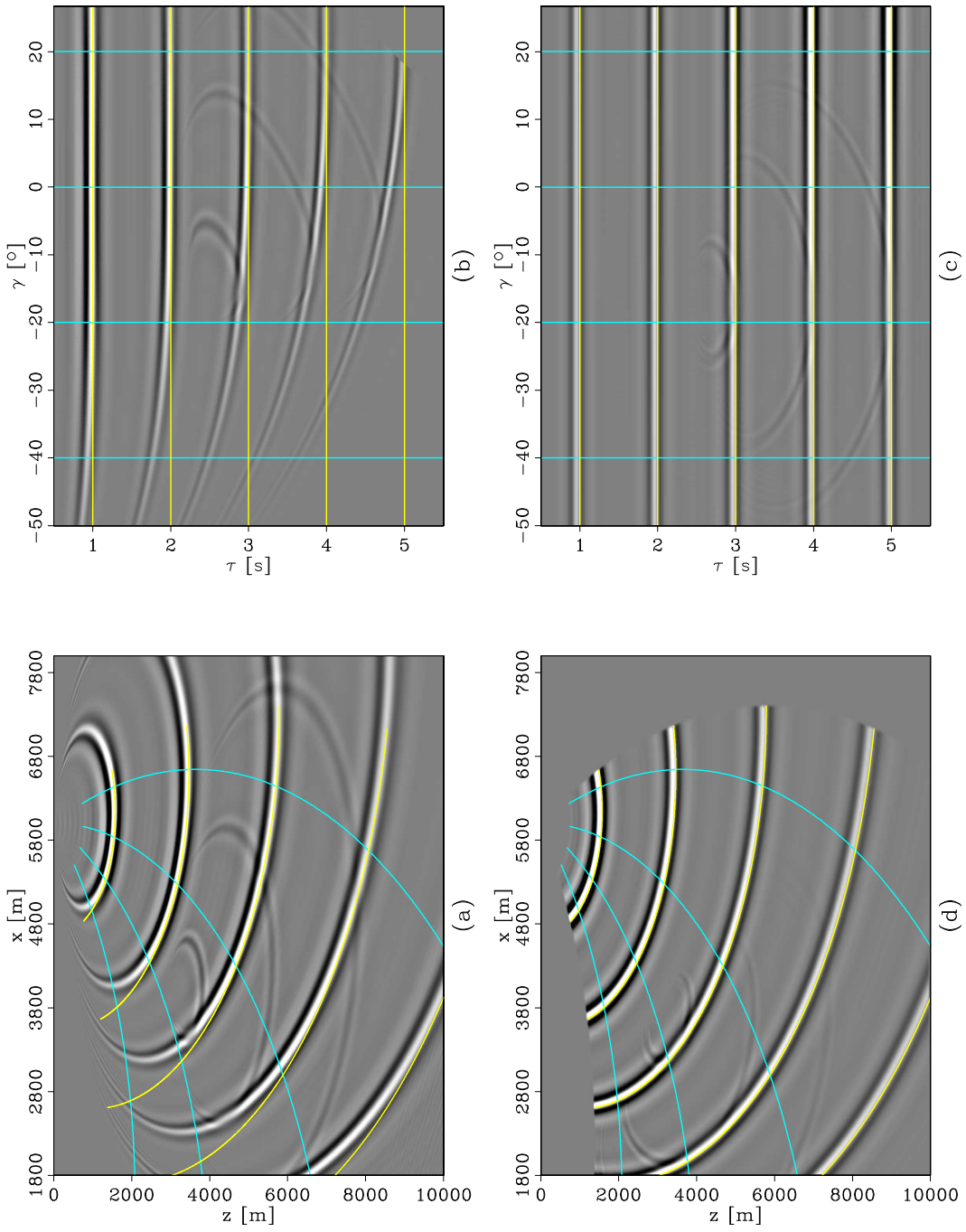

Figure 3: Simple linear gradient model: the image obtained by downward continuation in Cartesian coordinates with the 15° equation (a); the image in panel (a) interpolated to ray coordinates (b); image obtained by extrapolation in ray coordinates with the 15° equation (c); the image in panel (c) interpolated to Cartesian coordinates (d). paul2-RCsim.f15.ps [CR]

creates a triplication of the ray coordinate system (Figure 4). Everything other than the velocity model is identical to its counterpart in the preceding example. Similarly to Figure 2, panels (a) and (b) correspond to Cartesian coordinates, and panels (c) and (d) correspond to ray coordinates. Using regularization of the ray coordinates parameters, we are able to extrapolate through the triplication. The small discrepancy between the wavefields and the corresponding wavefronts indicate that our method of ray tracing is not perfectly accurate in the triplicating region, and the wavefield extrapolation is correcting for the kinematic differences. Figure 5 is similar to Figure 3. The "butterfly" in panel (b) is another indication that the ray coordinate system is triplicating, and different shooting directions pick up the same energy from the wavefield extrapolated in Cartesian coordinates (a). None of this happens when we extrapolate in ray coordinates (c) and interpolate to Cartesian coordinates (d).

Our next example concerns the more complicated Marmousi model. Figure 6 shows the velocity models mapped into the two different domains, and the wavefields obtained by extrapolation in each one of them. We create the ray coordinate system by ray tracing in a smooth version of the model, and extrapolate in the rough version. The source is located on the surface at $x = 5000$ m.

In this example, the wavefields triplicate in both domains (Figure 7). Since we are using a 15° equation, extrapolation in Cartesian coordinates is only accurate for the small incidence angles, as can be seen in panels (a) and (b). In contrast, extrapolating in ray coordinates (c) does not have the same angle limitation, which can also be seen after mapping back to Cartesian coordinates (d).

Figure 8 is a close-up comparison of the wavefields obtained by extrapolation with different methods in different domains. Panel (a) is a window of the velocity model for reference. Panels (b) and (c) are obtained by extrapolation in ray coordinates using the 15° and split-step equations, respectively. Panels (d), (e) and (f) are obtained by downward continuation in Cartesian coordinates using the 45°, 15° and split-step equations, respectively. The ray coordinates extrapolation results are similar to the Cartesian coordinates results in the regions where the wavefields propagate mostly vertically, but are much better in the regions where the wavefields propagate almost horizontally.

Next, we present another example in the Sigsbee 2A model. We consider two types of ray coordinates: one initiated by a plane wave at the surface (Figure 9), and one initiated by a point source at the surface at $x = 16000$ m. (Figure 10). Similarly to the preceding examples, we observe complicated wavefield propagation, with many triplications, of the extrapolated wavefields.

Figure 11 is a close-up comparison of the wavefields obtained by extrapolation with different methods in different domains. Panel (a) is a window of the velocity model for reference. Panel (b) is the wavefield obtained by finite-difference modeling using the two-way acoustic wave equation. This panel contains not only waves propagating forward, but also reflections which are not going to be modeled in the one-way extrapolation results. Panel (c) is obtained by downward continuation in Cartesian coordinates using the 45° equation, and panel (d) is obtained by extrapolation in ray coordinates using the 15° equation. We can observe good match of the forward propagating wavefields in (b) and (d), in contrast to the poor match with

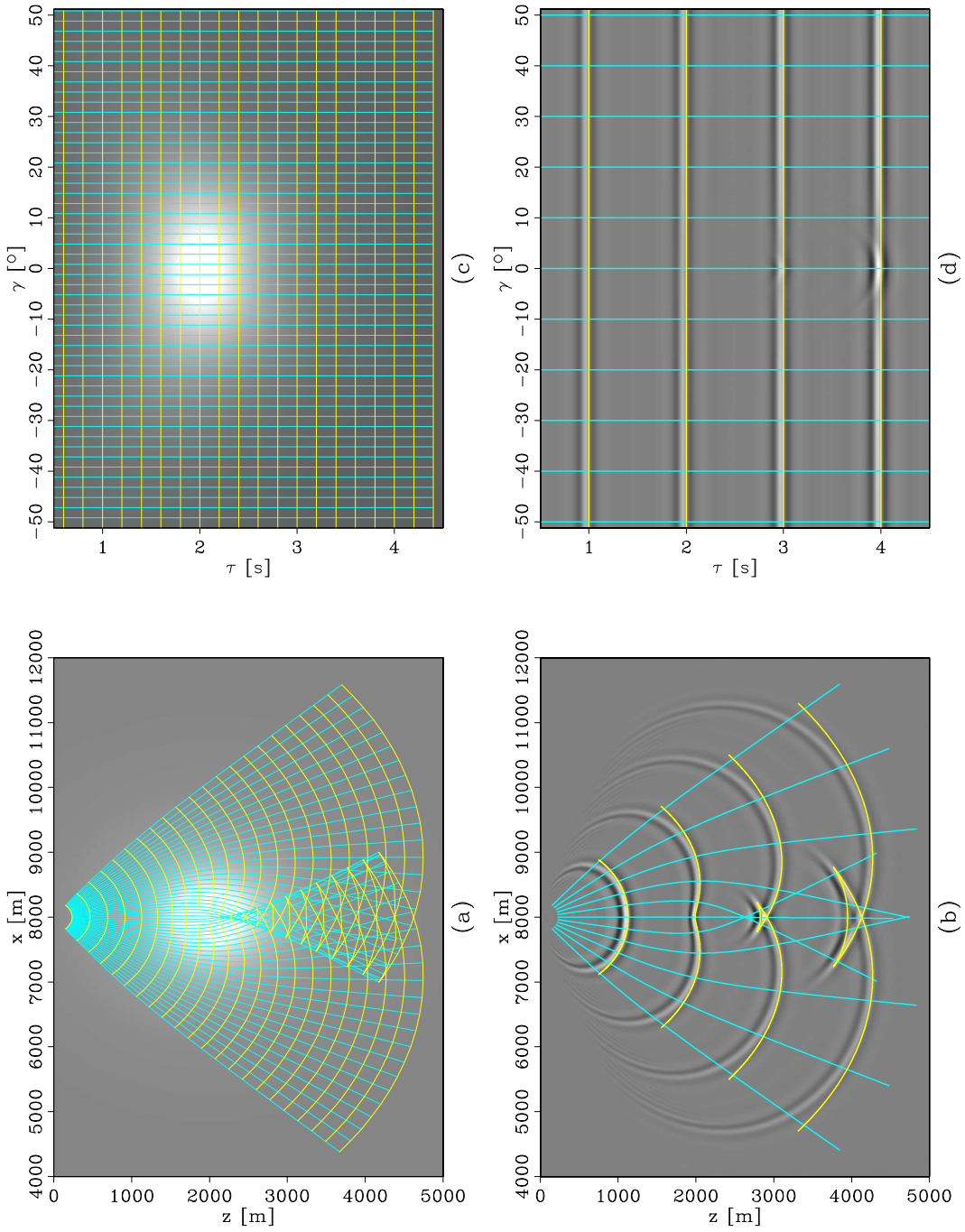

Figure 4: Gaussian anomaly model: Cartesian coordinates (a,b) and ray coordinates (c,d). velocity model with an overlay of the ray coordinate system initiated by a point source at the surface (a); image obtained by downward continuation in Cartesian coordinates with the 15° equation (b); velocity model with an overlay of the ray coordinate system (c); image obtained by wavefield extrapolation in ray coordinates with the 15° equation (d). paul2-RCga1.com.ps [CR]

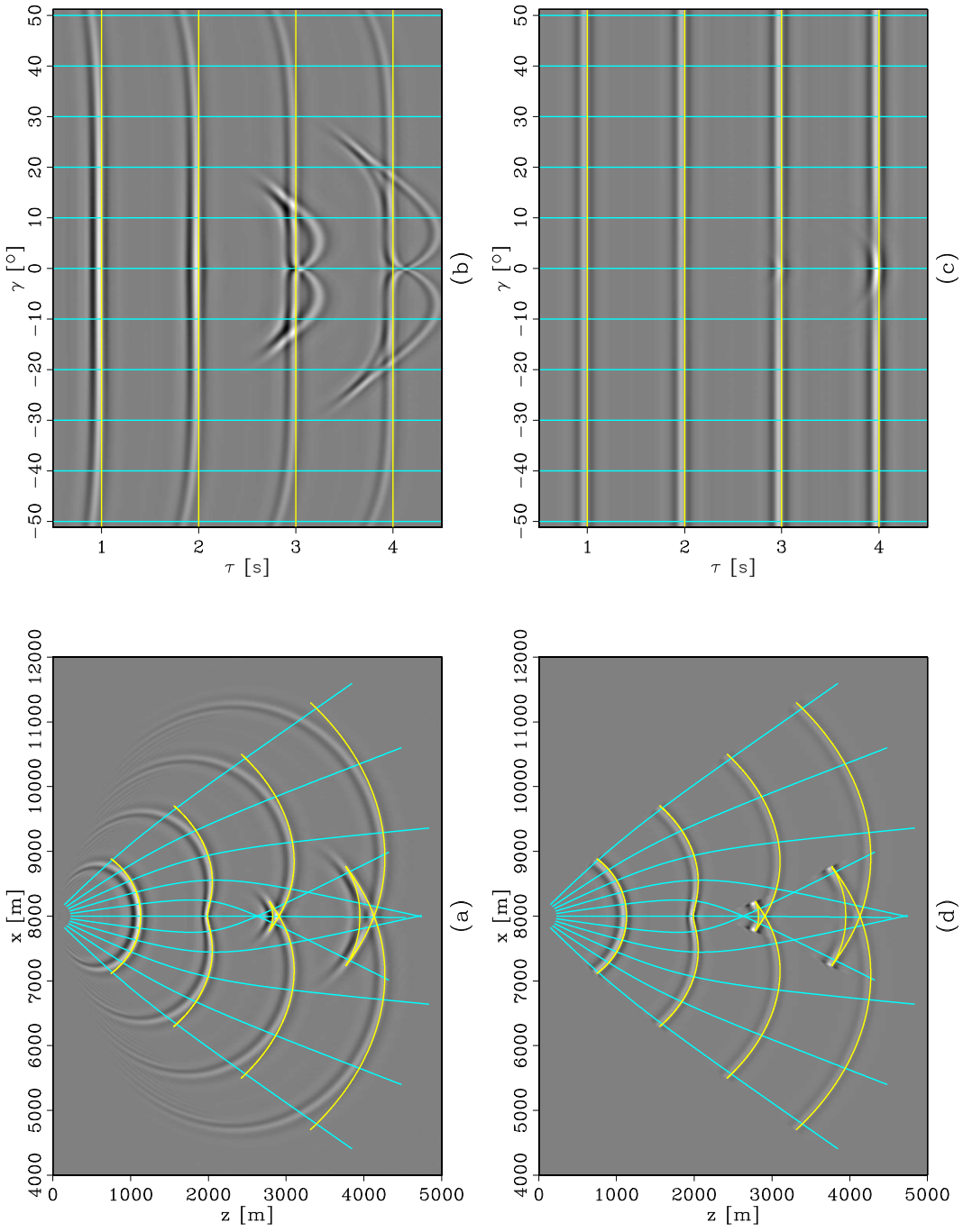

Figure 5: Gaussian anomaly model: the image obtained by downward continuation in Cartesian coordinates with the 15° equation (a); the image in panel (a) interpolated to ray coordinates (b); image obtained by extrapolation in ray coordinates with the 15° equation (c); the image in panel (c) interpolated to Cartesian coordinates (d). paul2-RCga1.f15.ps [CR]

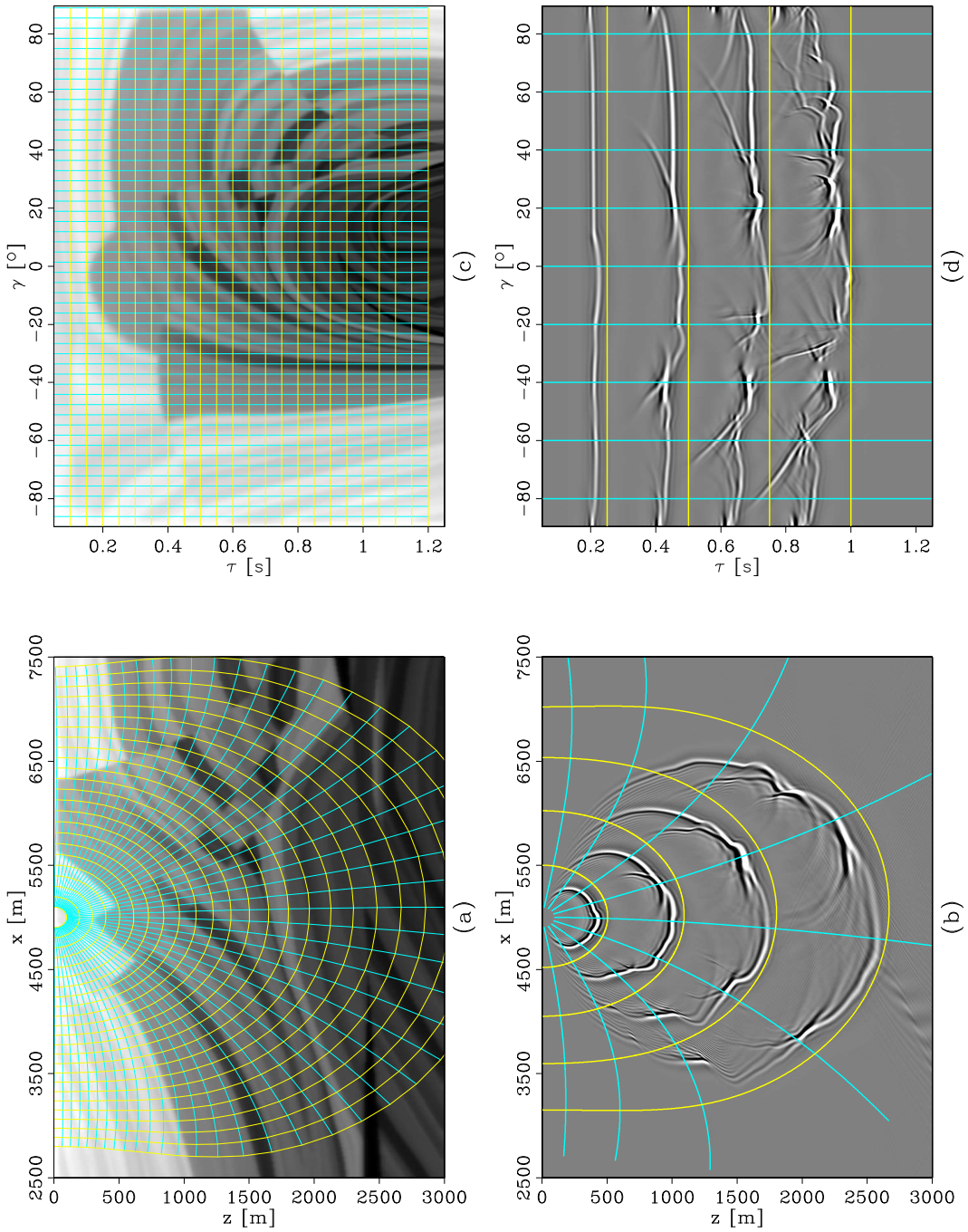

Figure 6: Marmousi model: Cartesian coordinates (a,b) and ray coordinates (c,d). velocity model with an overlay of the ray coordinate system initiated by a point source at the surface (a); image obtained by downward continuation in Cartesian coordinates with the 15° equation (b); velocity model with an overlay of the ray coordinate system (c); image obtained by wavefield extrapolation in ray coordinates with the 15° equation (d). paul2-RCma1.com.ps [CR]

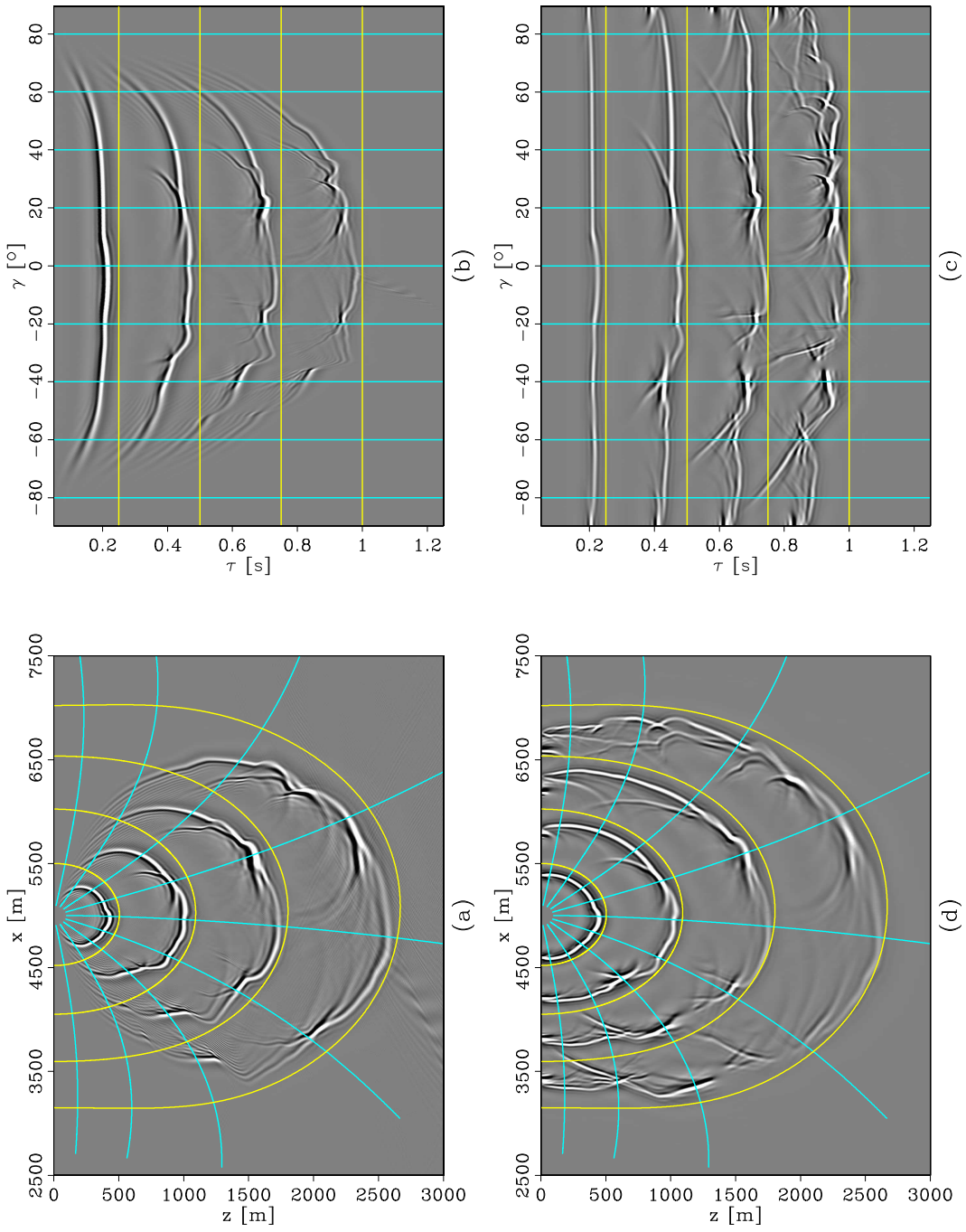

Figure 7: Marmousi model: the image obtained by downward continuation in Cartesian coordinates with the 15° equation (a); the image in panel (a) interpolated to ray coordinates (b); image obtained by extrapolation in ray coordinates with the 15° equation (c); the image in panel (c) interpolated to Cartesian coordinates (d). paul2-RCma1.f15.ps [CR]

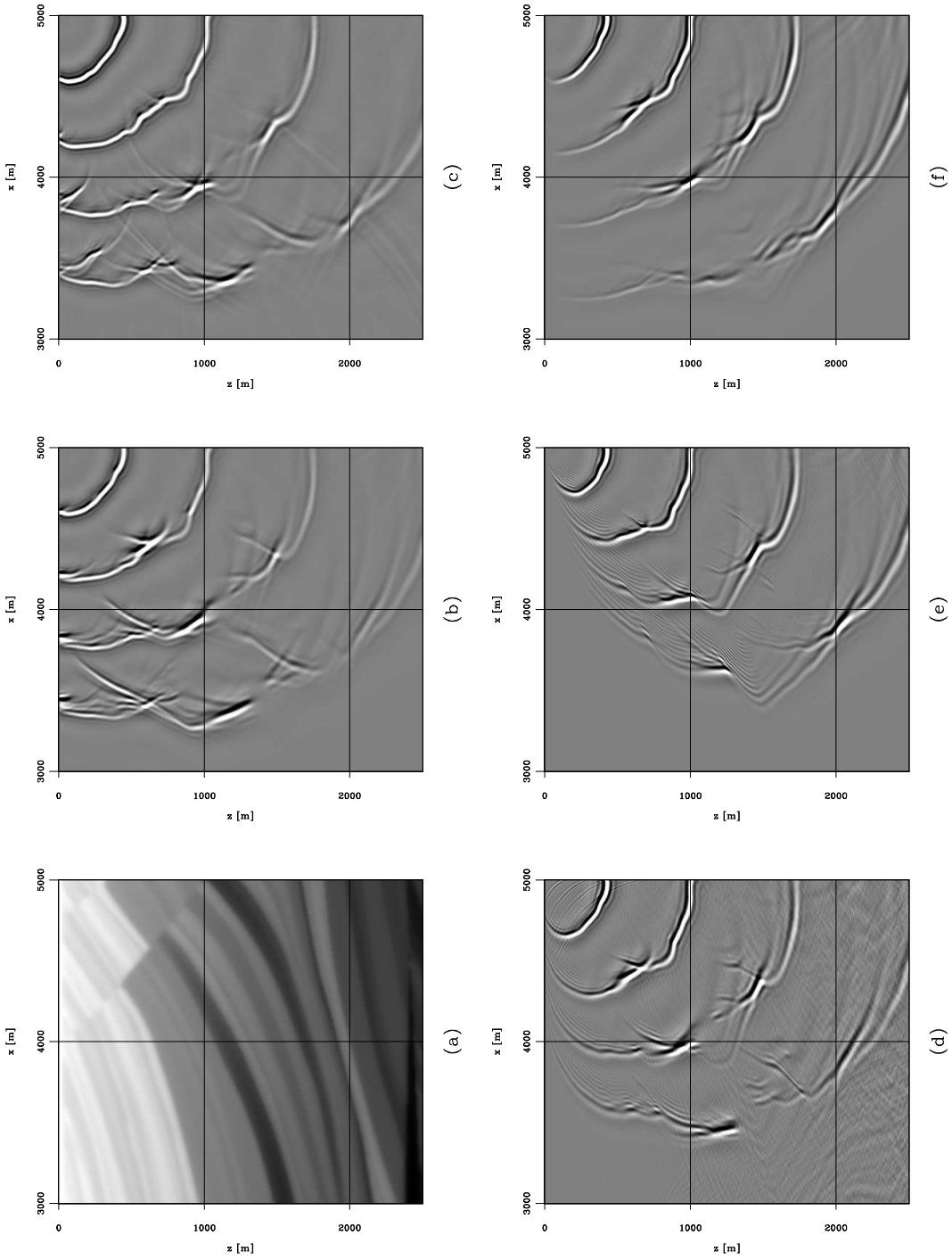

Figure 8: Marmousi model: Velocity model (a); image obtained by wavefield extrapolation in ray coordinates using the 15° equation (b) and the split-step equation (c); image obtained using downward continuation in Cartesian coordinates with the 45° equation (d), the 15° equation (e) and the split-step equation (f). paul2-RCma1.zom.ps [CR,M]

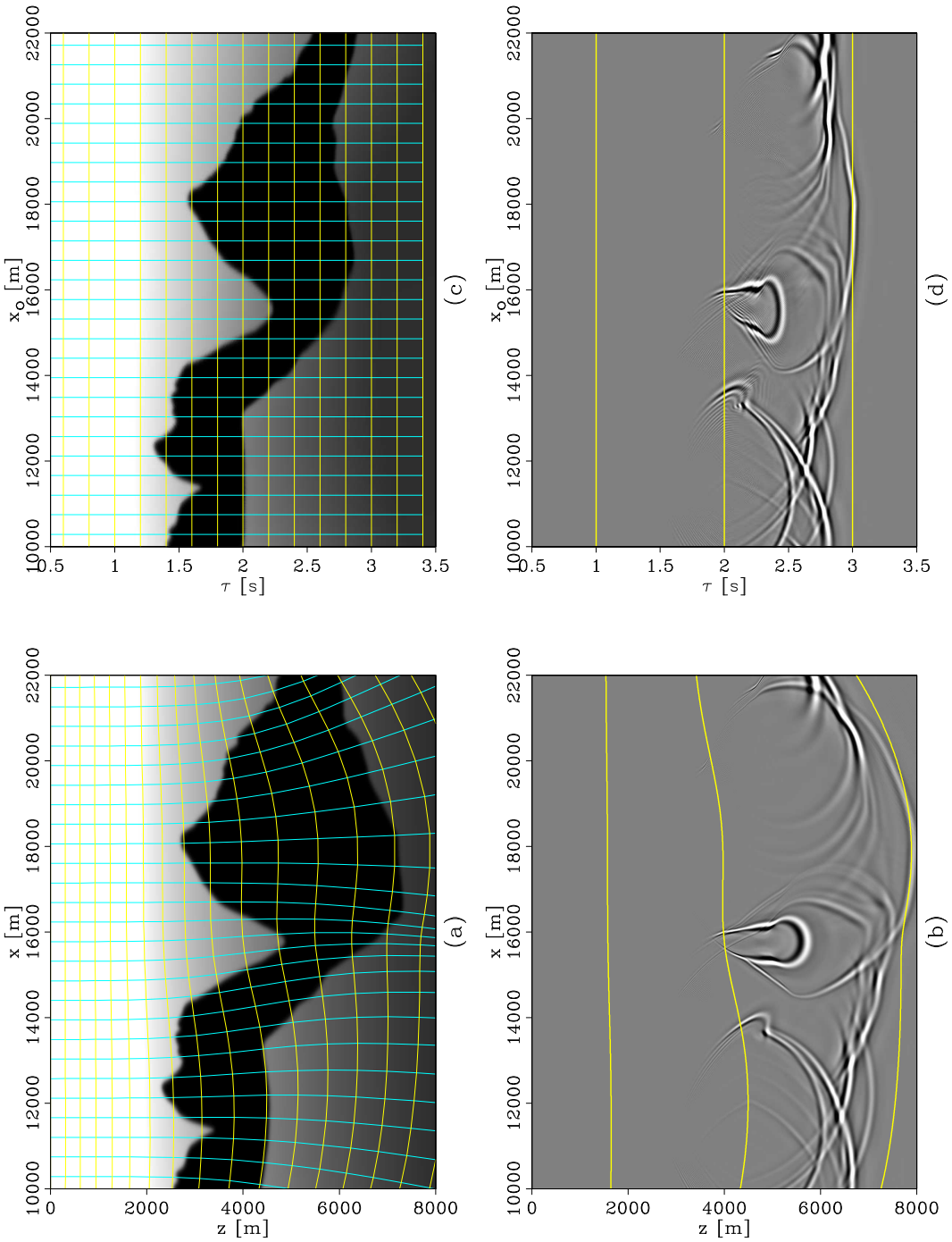

Figure 9: Sigsbee 2A model: Cartesian coordinates (a,b) and ray coordinates (c,d). velocity model with an overlay of the ray coordinate system initiated by a plane source at the surface (a); image obtained by downward continuation in Cartesian coordinates with the 15° equation (b); velocity model with an overlay of the ray coordinate system (c); image obtained by wavefield extrapolation in ray coordinates with the 15° equation (d). paul2-RCzg2.com.pw [CR]

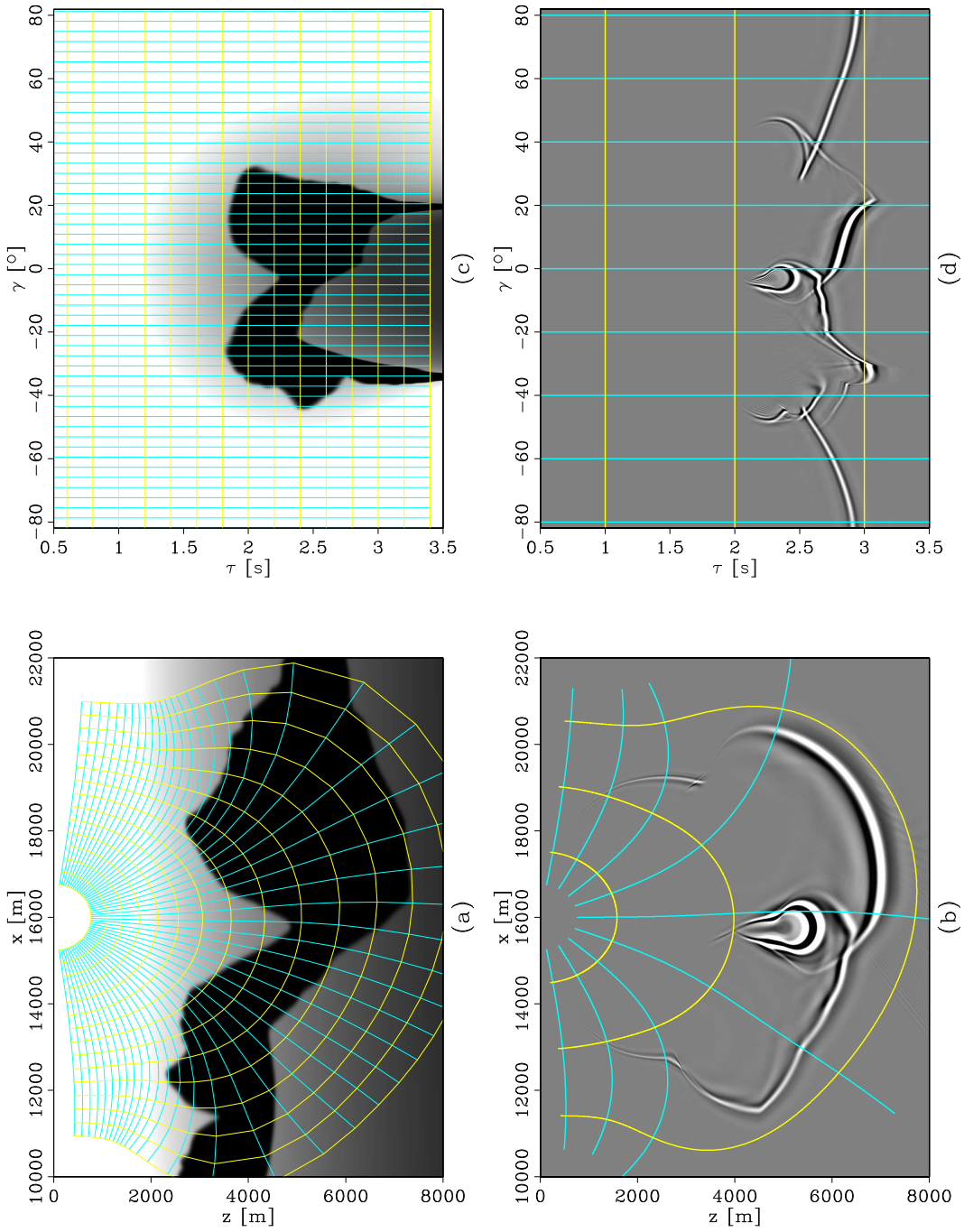

Figure 10: Sigsbee 2A model: Cartesian coordinates (a,b) and ray coordinates (c,d). velocity model with an overlay of the ray coordinate system initiated by a point source at the surface (a); image obtained by downward continuation in Cartesian coordinates with the 15° equation (b); velocity model with an overlay of the ray coordinate system (c); image obtained by wavefield extrapolation in ray coordinates with the 15° equation (d). paul2-RCzg2.com.ps [CR]

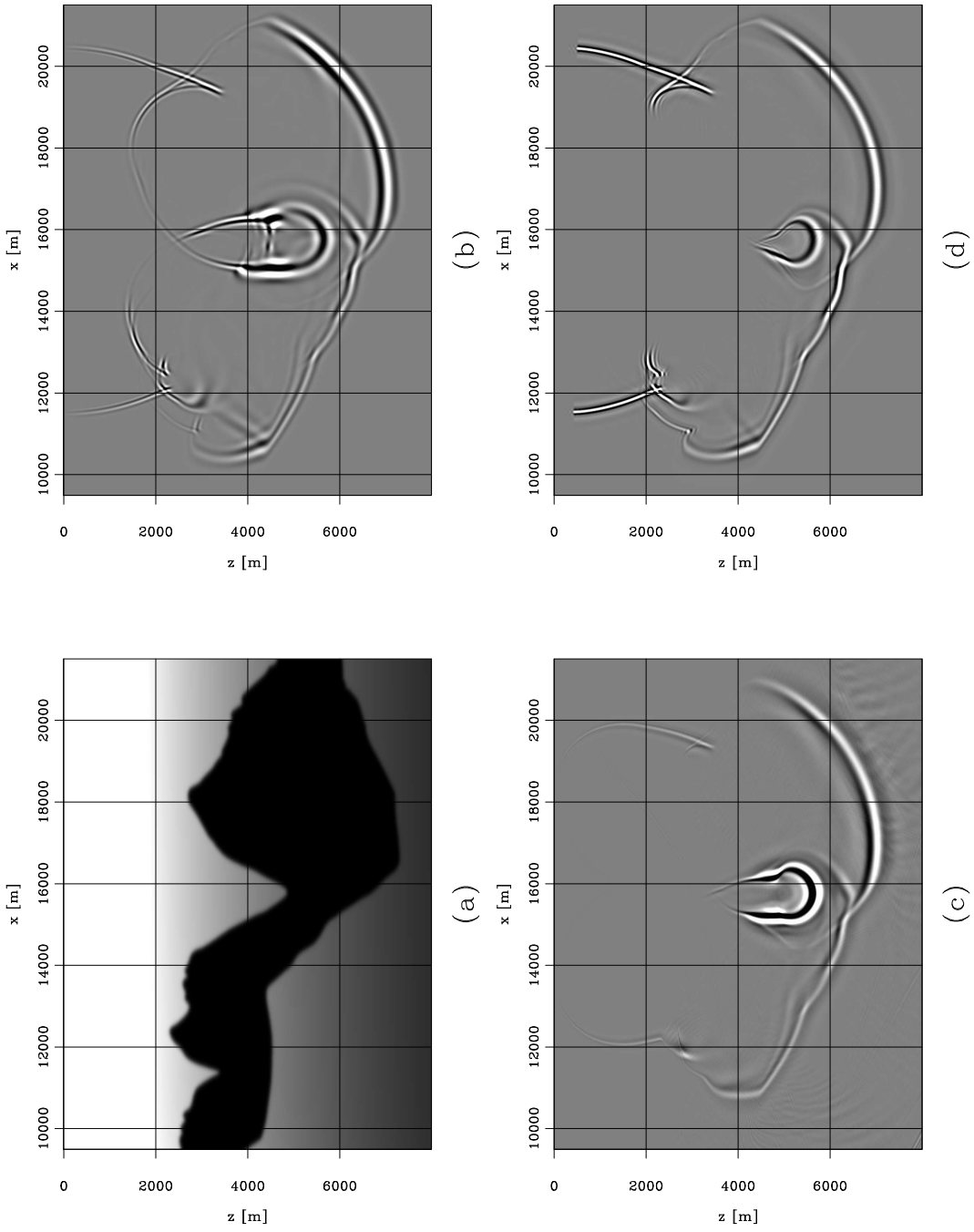

Figure 11: Sigsbee 2A model: Velocity (a); finite-difference solution to the two-way acoustic wave equation for a point source at $x = 16000$ m (b); image obtained by downward continuation in Cartesian coordinates with the 45° equation (c); image obtained by wavefield extrapolation in ray coordinates with the 15° equation (d). paul2-RCzg2.zom.ps [CR,M]

panel (c) in the regions of nearly horizontal propagation.

Finally, we present an example of zero-offset migration of overturning reflections using Riemannian wavefield extrapolation. Figure 12 depicts the velocity model (a), the recorded data (b), and the migrated image (c). The overlay is a sketch of the ray coordinate system used for migration. The first event in the data corresponds to the overturning reflection from the ball and is imaged correctly, and the later events are multiple reverberations inside the ball which are not imaged with our method.

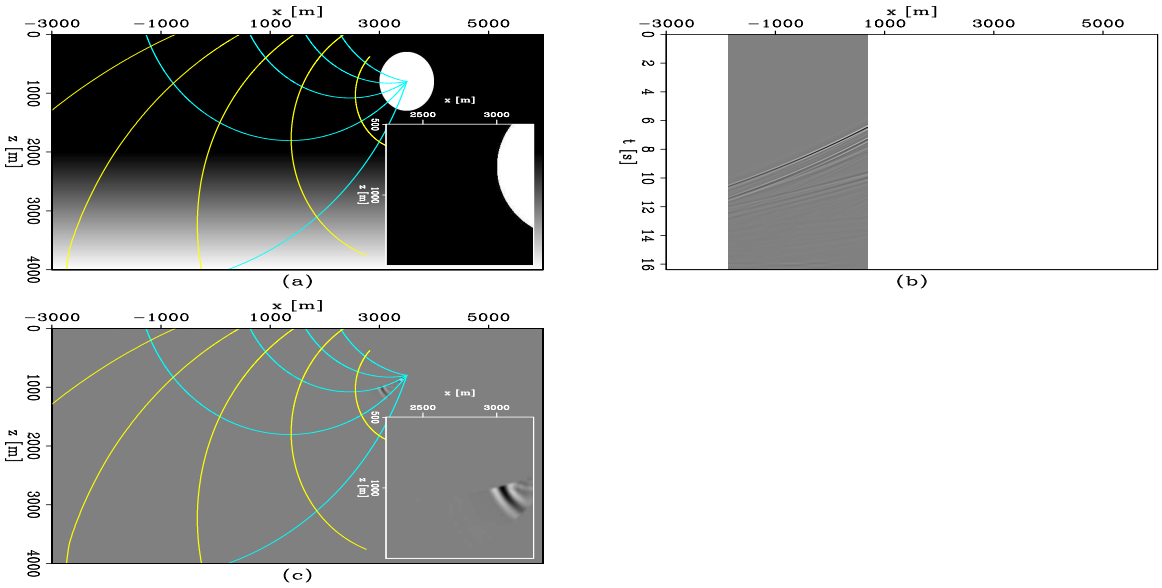

Figure 12: Imaging of overturning reflections using Riemannian wavefield extrapolation. Velocity model (a), zero-offset data (b), and migrated image (c). paul2-RCba1.ovt [CR,M]

KINEMATIC EXTRAPOLATION IN RIEMANNIAN COORDINATES

We can simplify our Riemannian wavefield extrapolation method by dropping the first order terms in equation (12). According to the theory of second-order hyperbolic equations, these terms affect only the amplitude of the propagating waves. To preserve the kinematics, it is sufficient to keep only the second order terms of equation (12):

$$k_\zeta = \pm\sqrt{\frac{(\omega s)^2}{c_{\zeta\zeta}} - \frac{c_{\xi\xi}}{c_{\zeta\zeta}}k_\xi^2 - \frac{c_{\eta\eta}}{c_{\zeta\zeta}}k_\eta^2 - \frac{c_{\xi\eta}}{c_{\zeta\zeta}}k_\xi k_\eta}\ . \tag{24}$$

Figure 13 illustrates the difference between wavefield extrapolation using equation (12) (panel b) and wavefield extrapolation using equation (24) (panel c). Kinematically, the two images are equivalent and the main changes are related to amplitudes.

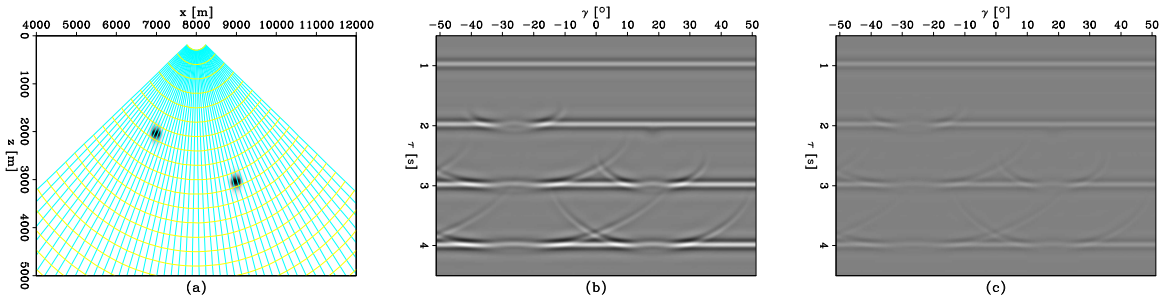

Figure 13: The effect of neglecting the first order terms in Riemannian wavefield extrapolation. From left to right the velocity model with an overlay of the ray coordinate system (a), extrapolation with equation (12) including the first order terms (b), and extrapolation with the simplified equation (24) (c). paul2-RCga2.kin.ps [CR]

DISCUSSION

We now present a few issues that we think are important for our Riemannian wavefield extrapolation method. In some cases, we discuss ideas which we have not treated yet, while in other cases we speculate on directions of future research.

3-D Riemannian extrapolation: All our examples of Riemannian extrapolation in 2-D using finite-differences use implicit methods, since they are more stable and there is no reason not to use them. In 3-D, however, implicit solutions to the one-way wave-equation become much more difficult, even in Cartesian coordinates (Fomel and Claerbout, 1997; Rickett et al., 1998). This problem seems even more complicated for Riemannian wavefield extrapolation, since the extrapolation equation also contains mixed $k_\xi k_\eta$ terms. However, we speculate that for wavefield extrapolation in ray coordinates, this problem is not as difficult as it seems at first sight. The reason is that energy propagates roughly in the forward direction of the coordinate system and, therefore, we do not need extrapolators accurate at high dips. Thus, we could either use explicit methods with reasonably small stencils, or we could use low order mixed-domain methods from the split-step family which are easy to implement even in 3-D.

Prestack data: Our examples of Riemannian wavefield extrapolation are based on equation (12) which corresponds to the single-square root (SSR) equation of standard Cartesian wavefield extrapolation. Riemannian wavefield extrapolation can be extended to prestack data either for shot-profile, plane-wave or S-G migration by appropriate definitions of the underlying ray coordinate system. Figure 14 is a schematic representation of shot-profile migration in ray coordinates, where both source and receivers are extrapolated in the same ray coordinate system appropriate for overturning waves. However, the sources and receivers do not necessarily have to be migrated in the same coordinate system. We could extrapolate both sides differently and apply the imaging condition after interpolation to the Cartesian grid.

Time wave-equation migration: Our Riemannian wavefield extrapolation allows the output

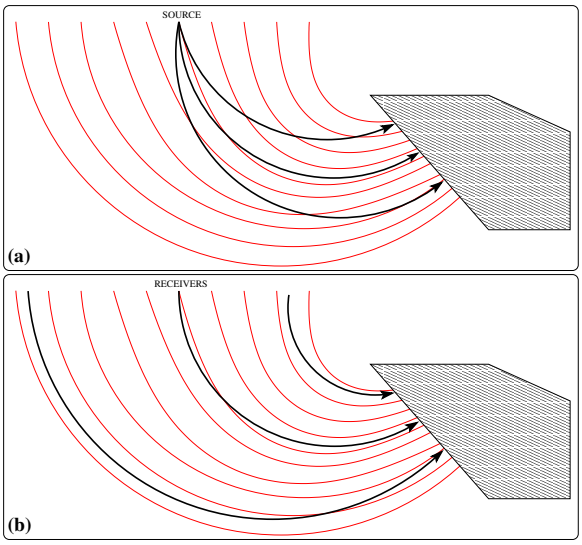

Figure 14: Shot-profile migration sketch. Sources (a) and receivers (b) are extrapolated in the same ray coordinate system which is appropriate for overturning waves. paul2-spmig [NR]

image to be presented either in one-way traveltime, which is the extrapolation coordinate, or in depth, after interpolation to Cartesian coordinates. A ray coordinate system initiated by a plane wave propagating vertically is related to what has been known in the literature as a "τ coordinate system" (Biondi et al., 1997; Alkhalifah et al., 2001). However, our τ ray coordinate system is different, because it allows energy to move laterally, in contrast to the vertical traveltime coordinate system which does not allow such movement. Thus, another application of Riemannian wavefield extrapolation is *time wave-equation migration* (Figure 9), which has interesting properties, e.g., for migration velocity analysis (Clapp, 2001). Furthermore, wave-equation MVA (Biondi and Sava, 1999; Sava and Fomel, 2002) could also be reformulated as a function of one-way propagation time.

Regularization at caustics: The coordinate system coefficients for Riemannian wavefield extrapolation given by equations (8) have singularities at caustics, e.g., when the geometrical spreading term J, defining a cross-sectional area of a ray tube, goes to zero. In our current examples, we have used simple numerical regularization, by adding a small non-zero quantity to the denominators to avoid division by zero. This strategy worked reasonably well for our current examples.

Adaptive grid: A potential difficulty of our method is represented by the uneven sampling of the wavefronts caused by focusing and defocussing of the rays defining the coordinate system. One solution to this problem is to use adaptive gridding, by increasing or decreasing sampling along the wavefronts, similarly to the techniques employed by the wavefront construction method (Vinje et al., 1993; Qian and Symes, 2002). Furthermore, each frequency in the data can be extrapolated on its own grid, sparser at lower frequencies and denser at higher frequency, thus reducing cost and increasing accuracy.

Interpolation: The images created with wavefield extrapolation in ray coordinates require interpolation to a Cartesian coordinate system. This is a shared difficulty of all methods that do not operate on a Cartesian grid. In our examples, we have successfully used a

simple sinc-type interpolation method. In principle, we could use better interpolation methods using prediction-error filters at higher cost, although we have not seen the need for this in our current examples.

Coordinate system construction: The ray coordinate systems do not need to be created using the same velocity model as the one used for extrapolation. We can use a smooth velocity model to create the coordinate system by ray tracing, and then interpolate the unsmoothed velocity, similarly to the method used by Brandsberg-Dahl and Etgen (2003). Such a strategy opens up the possibility of defining coordinate systems using arbitrary velocity models which favor selected parts of the image. For example, we could use for ray tracing a velocity model optimized to reduce, in a least-squares sense, the angle between the extrapolation grid and the dips in the image. An alternative method of creating ray coordinate systems is discussed by Shragge and Biondi (2003).

Amplitude preservation: Amplitude-preserving imaging using one-way wavefield extrapolation operators is difficult. Recent research has advanced our knowledge on this subject (Zhang et al., 2001; Sava et al., 2001; Shan and Biondi, 2003), but the goal of true-amplitude wave-equation migration is still unachieved. The biggest practical difficulty is associated with amplitude preservation at high scattering angles relative to the extrapolation direction. Since we are normally using low angle operators relative to the wave propagation direction, we speculate that Riemannian extrapolation can also improve the amplitude characteristics of wave-equation migration.

CONCLUSIONS

We extend one-way wavefield extrapolation to Riemannian spaces which are, by definition, described by non-orthogonal curvilinear coordinate systems. We choose semi-orthogonal Riemannian coordinates which include, but are not limited to, ray coordinate systems.

We define an acoustic wave-equation for semi-orthogonal Riemannian coordinates, from which we derive a one-way wavefield extrapolation equation. We use ray coordinates initiated either from a point source, or from an incident plane wave at the surface. Many other types of coordinates are acceptable, as long as they fulfill the semi-orthogonal condition of our acoustic wave equation.

Since wavefield propagation happens mostly along the extrapolation direction, we can use cheap 15° finite-difference or mixed-domain extrapolators to achieve high angle accuracy. If the ray coordinate system overturns, our method can be used to image overturning waves with one-way wavefield extrapolation.

A special case of extrapolation corresponds to coordinates initiated by a plane wave at the surface propagating initially in the vertical direction. Since our extrapolation is done as a function of one-way traveltime, this case resembles imaging in vertical traveltime, although it is more physically correct, since it allows lateral movement of energy, which is not the case for vertical τ imaging.

Two main applications of our method are imaging of steeply dipping or overturning reflections.

REFERENCES

Albertin, U., Yingst, D., and Jaramillo, H., 2001, Comparing common-offset Maslov, Gaussian beam, and coherent state migrations: 71st Ann. Internat. Mtg., Soc. of Expl. Geophys., Expanded Abstracts, 913–916.

Albertin, U., Yingst, D., Jaramillo, H., Wiggins, W., Chapman, C., and Nichols, D., 2002, Towards a hybrid raytrace-based beam/wavefield-extrapolated beam migration algorithm: 72nd Ann. Internat. Mtg, Soc. of Expl. Geophys., Expanded Abstracts, 1344–1347.

Alkhalifah, T., Fomel, S., and Biondi, B., 2001, The space-time domain: theory and modelling for anisotropic media: Geophysical Journal International, **144**, 105–113.

Biondi, B., and Sava, P., 1999, Wave-equation migration velocity analysis: 69th Ann. Internat. Meeting, Soc. of Expl. Geophys., Expanded Abstracts, 1723–1726.

Biondi, B., Fomel, S., and Alkhalifah, T., 1997, "Focusing" eikonal equation and global tomography: SEP–**95**, 61–76.

Biondi, B., 2002, Stable wide-angle Fourier finite-difference downward extrapolation of 3-D wavefields:, **67**, no. 03, 872–882.

Brandsberg-Dahl, S., and Etgen, J., 2003, Beam-wave migration: 65th Mtg., Eur. Assoc. Geosc. Eng., Abstracts.

Chen, L., Chen, Y., and Wu, R., 2002, Target-oriented prestack beamlet migration using Gabor-Daubechies frames: 72nd Ann. Internat. Mtg, Soc. of Expl. Geophys., Expanded Abstracts, 1356–1359.

Claerbout, J. F., 1985, Imaging the Earth's Interior: Blackwell Scientific Publications.

Clapp, R. G., 2001, Geologically constrained migration velocity analysis: Ph.D. thesis, Stanford University.

de Hoop, M. V., 1996, Generalization of the Bremmer coupling series: J. Math. Phys., 3246–3282.

Etgen, J., 2002, Waves, beams and dimensions: an illuminating if incoherent view of the future of migration: 72nd Ann. Internat. Mtg, Soc. of Expl. Geophys., invited presentation.

Fomel, S., and Claerbout, J. F., 1997, Exploring three-dimensional implicit wavefield extrapolation with the helix transform: SEP–**95**, 43–60.

Gazdag, J., and Sguazzero, P., 1984, Migration of seismic data by phase-shift plus interpolation: Geophysics, **49**, no. 2, 124–131.

Gray, S., Notfors, C., and Bleistein, N., 2002, Imaging using multi-arrivals: Gaussian beams or multi-arrival Kirchhoff?: 72nd Ann. Internat. Mtg, Soc. of Expl. Geophys., Expanded Abstracts, 1117–1120.

Hale, D., Hill, N. R., and Stefani, J., 1992, Imaging salt with turning seismic waves: Geophysics, **57**, no. 11, 1453–1462.

Hale, D., 1991, Stable explicit depth extrapolation of seismic wavefields: Geophysics, **56**, no. 11, 1770–1777.

Hill, N. R., 1990, Gaussian beam migration: Geophysics, **55**, no. 11, 1416–1428.

Hill, N. R., 2001, Prestack Gaussian-beam depth migration: Geophysics, **66**, no. 4, 1240–1250.

Huang, L. Y., and Wu, R. S., 1996, Prestack depth migration with acoustic screen propagators: 66th Ann. Internat. Mtg, Soc. Expl. Geophys., Expanded Abstracts, 415–418.

Nichols, D., and Palacharla, G., 1994, Band-limited Green's functions in 3-D: SEP–**80**, 17–24.

Nichols, D. E., 1994, Imaging complex structures using band-limited Green's functions: Ph.D. thesis, Stanford University.

Nichols, D. E., 1996, Maximum energy traveltimes calculated in the seismic frequency band: Geophysics, **61**, no. 01, 253–263.

Qian, J., and Symes, W. W., 2002, Finite-difference quasi-P traveltimes for anisotropic media:, **67**, no. 1, 147–155.

Rickett, J., Claerbout, J., and Fomel, S., 1998, Implicit 3-D depth migration by wavefield extrapolation with helical boundary conditions: 68th Ann. Internat. Meeting, Soc. of Expl. Geophys., Expanded Abstracts, 1124–1127.

Rietveld, W. E. A., and Berkhout, A. J., 1994, Prestack depth migration by means of controlled illumination: Geophysics, **59**, no. 05, 801–809.

Ristow, D., and Ruhl, T., 1994, Fourier finite-difference migration: Geophysics, **59**, no. 12, 1882–1893.

Sava, P., and Fomel, S., 2001, 3-D traveltime computation using Huygens wavefront tracing: Geophysics, **66**, no. 3, 883–889.

Sava, P., and Fomel, S., 2002, Wave-equation migration velocity analysis beyond the Born approximation: 72nd Ann. Internat. Mtg., Soc. of Expl. Geophys., Expanded Abstracts, 2285–2288.

Sava, P., Biondi, B., and Fomel, S., 2001, Amplitude-preserved common image gathers by wave-equation migration: 71st Ann. Internat. Mtg., Soc. of Expl. Geophys., Expanded Abstracts, 296–299.

Sava, P., 2000, A tutorial on mixed-domain wave-equation migration and migration velocity analysis: SEP–**105**, 139–156.

Shan, G., and Biondi, B., 2003, WKBJ and amplitude preserving one-way wave equation: SEP–**114**, 67–70.

Shragge, J., and Biondi, B., 2003, Wavefield extrapolation in phase-ray coordinates: SEP–**114**, 31–44.

Stoffa, P. L., Fokkema, J. T., de Luna Freire, R. M., and Kessinger, W. P., 1990, Split-step Fourier migration: Geophysics, **55**, no. 04, 410–421.

Synge, J. L., and Schild, A., 1978, Tensor calculus: Dover.

Červený, V., 2001, Seismic ray theory: Cambridge Univ. Press.

Vinje, V., Iversen, E., and Gjoystdal, H., 1993, Traveltime and amplitude estimation using wavefront construction: Geophysics, **58**, no. 08, 1157–1166.

Yedlin, M., 1981, The wave equation in ray-centered coordinates: SEP–**28**, 89–92.

Zhang, Y., Sun, J., Notfors, C., Bleistein, N., and Zhang, G., 2001, Towards accurate amplitudes for one-way wavefield extrapolation of 3-D common shot records: 71st Ann. Internat. Mtg., Soc. of Expl. Geophys., Workshop presentation.

APPENDIX A

WKBJ ASYMPTOTIC SOLUTIONS TO THE ACOUSTIC WAVE-EQUATION IN 3-D RIEMANNIAN SPACES

Neglecting wave propagation in the directions orthogonal to ζ, one can reduce the wave equation (6) to the form of the ordinary differential equation

$$\frac{1}{\alpha J}\frac{d}{d\zeta}\left(\frac{J}{\alpha}\frac{d\,\mathcal{U}}{d\zeta}\right)+\frac{\omega^2}{v^2}\,\mathcal{U}=\frac{1}{\alpha J}\frac{d(J/\alpha)}{d\zeta}\frac{d\,\mathcal{U}}{d\zeta}+\frac{1}{\alpha^2}\frac{d^2\,\mathcal{U}}{d\zeta^2}+\frac{\omega^2}{v^2}\,\mathcal{U}\approx 0\,. \tag{A-1}$$

The high-frequency (WKBJ) asymptotics for the solution of equation (A-1) can be obtained by using a trial solution $\mathcal{U}=A\,e^{i\,\omega\phi}$, substituting it in equation (A-1) and evaluating terms with the same order of ω. The highest asymptotic order yields an equation for the phase function ϕ:

$$-\frac{1}{\alpha^2}\left(\frac{d\,\phi}{d\zeta}\right)^2+\frac{\omega^2}{v^2}=0\,. \tag{A-2}$$

The next asymptotic order produces an equation for the amplitude function A:

$$\frac{1}{\alpha J}\frac{d(J/\alpha)}{d\zeta}\frac{d\,\phi}{d\zeta}\,A+\frac{2}{\alpha^2}\frac{d\,\phi}{d\zeta}\frac{d\,A}{d\zeta}+\frac{1}{\alpha^2}\frac{d^2\,\phi}{d\zeta^2}\,A=0\,. \tag{A-3}$$

Rearranging equation (A-2) to the form

$$\frac{d\,\phi}{d\zeta}=\pm\frac{\alpha}{v} \tag{A-4}$$

and equation (A-3) to the form

$$\frac{d(\log A)}{d\zeta}=-\frac{1}{2}\left[\frac{d\,(\log(J/\alpha))}{d\zeta}+\frac{d\,(\log(\alpha/v))}{d\zeta}\right], \tag{A-5}$$

we can solve them explicitly to obtain the WKBJ approximation for the wave traveling preferentially in the ζ direction:

$$\mathcal{U}_1\approx\mathcal{U}_0\left(\frac{v_1\,J_0}{v_0\,J_1}\right)^{1/2}\exp\left[\pm i\,\omega\int_{\zeta_0}^{\zeta_1}\frac{\alpha}{v}\,d\zeta\right] \tag{A-6}$$

In the case of the ray coordinate system, equation (A-6) corresponds to the Green's function approximation commonly employed in Kirchhoff imaging.

Accounting for the wave propagation in the directions different from ζ and constructing the solution numerically by finite differences allows us to account for the finite-bandwidth wave propagation effects.

APPENDIX B

2-D POINT-SOURCE RAY COORDINATES

For the case of 2-D point-source ray coordinates the acoustic wave equation (6) takes the form

$$\frac{1}{\alpha J}\left[\frac{\partial}{\partial \tau}\left(\frac{J}{\alpha}\frac{\partial \mathcal{U}}{\partial \tau}\right)+\frac{\partial}{\partial \gamma}\left(\frac{\alpha}{J}\frac{\partial \mathcal{U}}{\partial \gamma}\right)\right]=-\frac{\omega^2}{v^2(\tau,\gamma)}\mathcal{U}\,, \tag{B-1}$$

where, by definition,

$$\begin{aligned}\alpha &= \sqrt{\left(\frac{\partial z}{\partial \tau}\right)^2+\left(\frac{\partial x}{\partial \tau}\right)^2}=v\,,\\ J &= \sqrt{\left(\frac{\partial z}{\partial \gamma}\right)^2+\left(\frac{\partial x}{\partial \gamma}\right)^2}\,.\end{aligned} \tag{B-2}$$

The extrapolation axis is τ (one-way traveltime from the source) and γ is the shooting angle at the source.

We can expand the parentheses in equation (B-1)

$$\frac{1}{v^2}\frac{\partial^2 \mathcal{U}}{\partial \tau^2}+\frac{1}{vJ}\frac{\partial (J/v)}{\partial \tau}\frac{\partial \mathcal{U}}{\partial \tau}+\frac{1}{vJ}\frac{\partial (v/J)}{\partial \gamma}\frac{\partial \mathcal{U}}{\partial \gamma}+\frac{1}{J^2}\frac{\partial^2 \mathcal{U}}{\partial \gamma^2}=-\frac{\omega^2}{v^2(\tau,\gamma)}\mathcal{U} \tag{B-3}$$

and make the notations

$$\begin{aligned}c_{\tau\tau} &= \frac{1}{\alpha^2}\,,\\ c_{\tau} &= \frac{1}{\alpha J}\frac{\partial}{\partial \tau}\left(\frac{J}{\alpha}\right)\,,\\ c_{\gamma} &= \frac{1}{\alpha J}\frac{\partial}{\partial \gamma}\left(\frac{\alpha}{J}\right)\,,\\ c_{\gamma\gamma} &= \frac{1}{J^2}\,,\end{aligned} \tag{B-4}$$

from which the acoustic wave equation for 2-D point-source ray coordinates becomes:

$$c_{\tau\tau}\frac{\partial^2 \mathcal{U}}{\partial \tau^2}+c_{\tau}\frac{\partial \mathcal{U}}{\partial \tau}+c_{\gamma}\frac{\partial \mathcal{U}}{\partial \gamma}+c_{\gamma\gamma}\frac{\partial^2 \mathcal{U}}{\partial \gamma^2}=-\frac{\omega^2}{v^2}\mathcal{U}\,. \tag{B-5}$$

The 2-D dispersion relation is

$$-c_{\tau\tau}k_{\tau}^2+ic_{\tau}k_{\tau}+ic_{\gamma}k_{\gamma}-c_{\gamma\gamma}k_{\gamma}^2=-\omega^2 s^2\,, \tag{B-6}$$

from which we can obtain the one-way wave equation for 2-D point-source ray coordinates:

$$k_{\tau}=i\frac{c_{\tau}}{2c_{\tau\tau}}\pm\sqrt{\frac{(\omega s)^2}{c_{\tau\tau}}-\left(\frac{c_{\tau}}{2c_{\tau\tau}}\right)^2+i\frac{c_{\gamma}}{c_{\tau\tau}}k_{\gamma}-\frac{c_{\gamma\gamma}}{c_{\tau\tau}}k_{\gamma}^2}\,. \tag{B-7}$$

APPENDIX C

FINITE-DIFFERENCE SOLUTION TO THE 15° EQUATION

This appendix details the computations associated with the finite-difference solution to the 15° equation in a 2-D orthogonal Riemannian space. The 3-D wave equation (22) takes in two dimensions the simpler form:

$$k_\zeta \approx i\,\frac{c_\zeta}{2c_{\zeta\zeta}} + k_o + \frac{i\,c_\xi}{2c_{\zeta\zeta}\,k_o}k_\xi + \frac{1}{2\,k_o}\left[\left(\frac{c_\xi}{2c_{\zeta\zeta}\,k_o}\right)^2 - \frac{c_{\xi\xi}}{c_{\zeta\zeta}}\right]k_\xi^2\,. \tag{C-1}$$

If we substitute the Fourier-domain wavenumbers by their equivalent space-domain partial derivatives, we obtain

$$\frac{\partial \mathcal{U}}{\partial k_\zeta} \approx -\frac{c_\zeta}{2c_{\zeta\zeta}} + i\,k_o + \frac{i\,c_\xi}{2c_{\zeta\zeta}\,k_o}\frac{\partial \mathcal{U}}{\partial k_\xi} - \frac{i}{2\,k_o}\left[\left(\frac{c_\xi}{2c_{\zeta\zeta}\,k_o}\right)^2 - \frac{c_{\xi\xi}}{c_{\zeta\zeta}}\right]\frac{\partial^2 \mathcal{U}}{\partial k_\xi^2}\,. \tag{C-2}$$

A finite-difference implementation of equation (C-2) involving the Crank-Nicolson method is

$$\begin{aligned}\frac{\mathcal{U}_{\zeta+1}^{\xi}-\mathcal{U}_{\zeta}^{\xi}}{\Delta\zeta} &\approx \frac{i\,c_\xi}{2c_{\zeta\zeta}\,k_o}\frac{\left(\mathcal{U}_{\zeta}^{\xi+1}-\mathcal{U}_{\zeta}^{\xi-1}\right)+\left(\mathcal{U}_{\zeta+1}^{\xi+1}-\mathcal{U}_{\zeta+1}^{\xi-1}\right)}{4\Delta\xi} \\ -\frac{i}{2\,k_o}\left[\left(\frac{c_\xi}{2c_{\zeta\zeta}\,k_o}\right)^2 - \frac{c_{\xi\xi}}{c_{\zeta\zeta}}\right]&\frac{\left(\mathcal{U}_{\zeta}^{\xi-1}-2\mathcal{U}_{\zeta}^{\xi}+\mathcal{U}_{\zeta}^{\xi+1}\right)+\left(\mathcal{U}_{\zeta+1}^{\xi-1}-2\mathcal{U}_{\zeta+1}^{\xi}+\mathcal{U}_{\zeta+1}^{\xi+1}\right)}{2\Delta\xi^2}\,.\end{aligned} \tag{C-3}$$

If we make the notations

$$\begin{aligned}\mu &= \frac{i\,c_\xi}{2c_{\zeta\zeta}\,k_o}\frac{\Delta\zeta}{4\Delta\xi} \\ \nu &= -\frac{i}{2\,k_o}\left[\left(\frac{c_\xi}{2c_{\zeta\zeta}\,k_o}\right)^2 - \frac{c_{\xi\xi}}{c_{\zeta\zeta}}\right]\frac{\Delta\zeta}{2\Delta\xi^2}\,,\end{aligned} \tag{C-4}$$

we can write equation (C-3) as

$$\begin{aligned}\mathcal{U}_{\zeta+1}^{\xi}-\mathcal{U}_{\zeta}^{\xi} &\approx \mu\left(\mathcal{U}_{\zeta}^{\xi+1}-\mathcal{U}_{\zeta}^{\xi-1}+\mathcal{U}_{\zeta+1}^{\xi+1}-\mathcal{U}_{\zeta+1}^{\xi-1}\right) \\ &+ \nu\left(\mathcal{U}_{\zeta}^{\xi-1}-2\mathcal{U}_{\zeta}^{\xi}+\mathcal{U}_{\zeta}^{\xi+1}+\mathcal{U}_{\zeta+1}^{\xi-1}-2\mathcal{U}_{\zeta+1}^{\xi}+\mathcal{U}_{\zeta+1}^{\xi+1}\right)\,,\end{aligned} \tag{C-5}$$

or, if we isolate the terms corresponding to the two extrapolation levels as:

$$\begin{aligned}\mathcal{U}_{\zeta+1}^{\xi} &- \mu\left(\mathcal{U}_{\zeta+1}^{\xi+1}-\mathcal{U}_{\zeta+1}^{\xi-1}\right)-\nu\left(\mathcal{U}_{\zeta+1}^{\xi-1}-2\mathcal{U}_{\zeta+1}^{\xi}+\mathcal{U}_{\zeta+1}^{\xi+1}\right) = \\ \mathcal{U}_{\zeta}^{\xi} &+ \mu\left(\mathcal{U}_{\zeta}^{\xi+1}-\mathcal{U}_{\zeta}^{\xi-1}\right)+\nu\left(\mathcal{U}_{\zeta}^{\xi-1}-2\mathcal{U}_{\zeta}^{\xi}+\mathcal{U}_{\zeta}^{\xi+1}\right)\,.\end{aligned} \tag{C-6}$$

After grouping the terms, we obtain

$$-(\nu-\mu)\,\mathcal{U}_{\zeta+1}^{\xi-1}+(1+2\nu)\,\mathcal{U}_{\zeta+1}^{\xi}-(\nu+\mu)\,\mathcal{U}_{\zeta+1}^{\xi+1} = (\nu-\mu)\,\mathcal{U}_{\zeta}^{\xi-1}+(1-2\nu)\,\mathcal{U}_{\zeta}^{\xi}+(\nu+\mu)\,\mathcal{U}_{\zeta}^{\xi+1}\,, \tag{C-7}$$

which is a finite-difference representation of the 15° solvable using fast tridiagonal solvers.